Jahn-Teller transition in $La_{1-x}Sr_xMnO_3$ in the low-doping region ($0<x\leqslant 0.1$)

Tapan Chatterji,[1,2] Bachir Ouladdiaf,[1] P. Mandal,[3] B. Bandyopadhyay,[3] and B. Ghosh[3]
[1]*Institut Laue-Langevin, BP 156, 38042 Grenoble Cedex 9, France*
[2]*Max-Planck-Institut für Physik Komplexer Systeme, Dresden, Germany*
[3]*Saha Institute of Nuclear Physics, 1/AF Bidhannagar, Calcutta 700 064, India*
(Received 26 February 2002; revised manuscript received 4 June 2002; published 1 August 2002)

We have investigated the Jahn-Teller transition in $La_{1-x}Sr_xMnO_3$ by high-temperature powder neutron diffraction in the low-doping region ($0<x\leqslant 0.1$). The Jahn-Teller transition temperature which is about $T_{JT}\approx 750$ K for stoichiometric $LaMnO_3$ is drastically reduced on doping with Sr, becoming $T_{JT}\approx 475$ K for $x=0.10$. The previously identified metrically cubic orthorhombic *O* phase (*Pmnb*) for $x=0$ becomes clearly (also metrically) orthorhombic for small doping $x=0.05$ and remains so in the doping range investigated. The Jahn-Teller transition is accompanied only by the partial reduction of the distortion of the MnO_6 octahedra. From the distortion of the MnO_6 octahedra we have determined the orbital mixing coefficients.

DOI: 10.1103/PhysRevB.66.054403 PACS number(s): 61.12.Ld, 61.66.Fn

A huge amount of theoretical and experimental investigations has been undertaken recently on hole-doped manganites which show colossal magnetoresistance (CMR) effects.[1–4] Despite all these efforts, the microscopic origin of the CMR effect in manganites remains still controversial. The ferromagnetic ground state of the doped manganites and the CMR effect are qualitatively understood on the basis of strong Hund's coupling and the double-exchange (DE) mechanism. It has, however, been realized that the charge, spin, orbital, and lattice degrees of freedom are all involved in the physics of manganites. Undoped stoichiometric $LaMnO_3$, which is an antiferromagnetic insulator, has an orthorhombic *Pbnm* structure at room temperature and shows orbital ordering due to the strong collective Jahn-Teller (JT) interaction. It undergoes a structural phase transition at $T_{JT}\approx 750$ K, above which the orbital ordering disappears. The orbital ordering below the JT transition temperature consists of alternate staggered arrangements of $d_{3x^2-r^2}$ and $d_{3y^2-r^2}$ orbitals in the *a-b* plane of the orthorhombic *Pbnm* structure (Fig. 1). The orbital ordering along the *c* axis repeats the same pattern. This particular arrangement of the orbitals is responsible for strong ferromagnetic (FM) coupling in the *a-b* plane and weak antiferromagnetic (AFM) coupling along the *c* axis. Doping $LaMnO_3$ with divalent ions (holes) oxidizes Mn^{3+} ions to Mn^{4+} and transforms the antiferromagnetic insulating ground state to a ferromagnetic metal which shows large negative magnetoresistance effect close to T_C. The $La_{1-x}Sr_xMnO_3$ is the best example of a DE system. It has the largest one-electron bandwidth *W* and is therefore less affected by Coulomb correlation effects. However, the end compound $LaMnO_3$ ($x=0$), as we have already noted, is strongly affected by cooperative JT interaction. The electron correlation effect is strong because of $n=1$ filling of the e_g band. The JT transition temperature depends strongly on the Mn^{4+} concentration. It decreases drastically with *x* as has been observed by our resistivity measurements,[5] which show anomalies at the JT transition.

No systematic diffraction experiments has been performed so far to investigate the doping dependence of the JT transition in $La_{1-x}Sr_xMnO_3$. Neutron diffraction is very sensitive to detect distortions due to the orbital ordering and several important parameters related to this phenomenon can be deduced from this. Note that although anomalous synchrotron x-ray scattering has been claimed[6] to have given direct evidence of orbital ordering in $LaMnO_3$, in reality it also probes the lattice distortion associated with orbital ordering, but in the absence of proper interpretation, only qualitatively. Powder neutron diffraction on the other hand has yielded much more valuable and quantitative results on stoichiometric $LaMnO_3$.[7] The antiferrodistorsive orbital ordering is evidenced by the spatial distribution of the Mn-O bond lengths. In a detailed structural analysis using high-resolution neutron powder diffraction data on stoichiometric $LaMnO_3$, Rodriguez-Carvajal *et al.*[7] have shown that the phase above T_{JT}, although metrically cubic, has the same orthorhombic space group *Pbnm* of the low-temperature phase. The MnO_6 octahedra become nearly regular above T_{JT} and the thermal parameters of oxygen atoms increase significantly. The observed average cubic lattice is believed to be the result of dynamic spatial fluctuations of the underlying orthorhombic distortion. The orbital mixing coefficients of the orbitally ordered phase below T_{JT} have been determined as functions of temperature. The high-resolution neutron powder diffraction results of Rodriguez-Carvajal *et al.*[7] is a clear demonstration of the strength of this technique in determining the subtle electronic effects close to T_{JT}. It is highly desirable to perform similar investigations on $La_{1-x}Sr_xMnO_3$ for small doping and study the evolution of the orbital order as a function of doping. We have investigated the Jahn-Teller transition in $La_{1-x}Sr_xMnO_3$ in the small doping range ($0<x\leqslant 0.1$).

The powder samples of $La_{1-x}Sr_xMnO_3$ used in the present study were obtained by crushing single-crystal ingots. Such a procedure makes possible preparation of pure homogeneous polycrystalline materials. We have grown $La_{1-x}Sr_xMnO_3$ single crystals by the floating zone method using an image furnace in a flow of Ar in the low doping range ($0<x\leqslant 0.1$). The typical growth rate was 5 mm/h with a speed of rotation 30 rpm. The polycrystalline ceramic rods of several centimeters in length and about 5 mm in diameter

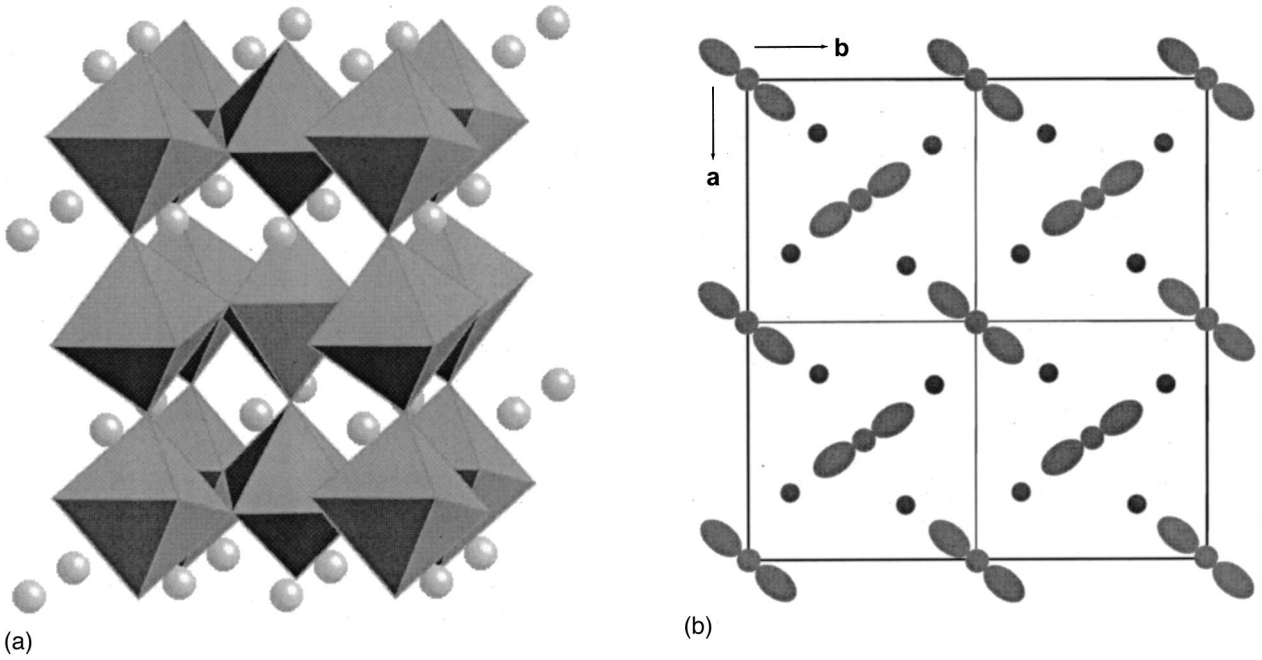

FIG. 1. (a) Schematic representation of the orthorhombic *Pbnm* crystal structure of $LaMnO_3$ in which La atoms and the MnO_6 octahedrons are shown. (b) Schematic representation of the orbital ordering in $LaMnO_3$ in the a-b plane. The orbital ordering below the JT transition temperature consists of alternate staggered arrangements of $d_{3x^2-r^2}$ and $d_{3y^2-r^2}$ orbitals in the a-b plane of the orthorhombic *Pbnm* structure. The Mn $d_{3x^2-r^2}$ and $d_{3y^2-r^2}$ orbitals and the O atoms are shown. The orbital ordering along the c axis repeats the same pattern.

were prepared by reacting high-purity ($\geqslant$99.99%) La_2O_3, $SrCO_3$, and Mn_3O_4 in appropriate ratios at high temperatures. The samples were characterized and the crystal quality was checked by x-ray powder diffractometry and the Laue technique. The high-temperature resistivity of the samples was measured[5] in Ar using a homemade apparatus. Neutron powder diffraction measurements were performed in the temperature range 293–873 K on the diffractometer D2B of

TABLE I. Structural parameters obtained by Rietveld refinements of the neutron powder diffraction data of $La_{1-x}Sr_xMnO_3$ for $x=0.05$ at several temperatures.

	$La_{1-x}Sr_xMnO_3$, $x=0.05$					
Space group	*Pbnm*	*Pbnm*	*Pbnm*	*Pbnm*	*Pbnm*	$R\bar{3}c$
T (K)	300	573	723	733	773	873
a (Å)	5.5335(5)	5.456(4)	5.5674(1)	5.5683(1)	5.5717(1)	5.58398(8)
b (Å)	5.6490(5)	5.5864(4)	5.5420(1)	5.5421(1)	5.5423(1)	
c (Å)	7.6981(7)	7.7936(6)	7.8529(2)	7.8537(2)	7.8559(2)	13.5062(2)
x (La)	−0.0078(9)	−0.0045(10)	−0.0023(5)	−0.0025(5)	−0.0026(6)	
y (La)	0.0381(8)	0.0289(6)	0.0177(3)	0.0177(3)	0.0172(4)	
B (LA) (Å^2)	0.85(7)	1.17(5)	1.37(3)	1.37(3)	1.38(3)	1.54(3)
B (Mn) (Å^2)	0.62(14)	0.78(10)	0.86(4)	0.81(4)	0.83(5)	1.06(5)
x (O1)	0.0726(10)	0.0718(9)	0.0692(5)	0.0697(5)	0.0691(6)	0.4434(2)
y (O1)	0.4908(10)	0.4899(9)	0.4924(6)	0.4931(6)	0.4918(8)	
B (O1) (Å^2)	0.70(10)	1.40(8)	1.86(5)	1.89(5)	1.86(6)	2.54(3)
x (O2)	0.7298(9)	0.7323(9)	0.7283(4)	0.7287(4)	0.7313(5)	
y (O2)	0.2974(7)	0.2892(6)	0.2739(4)	0.2738(4)	0.2732(4)	
z (O2)	0.0390(6)	0.0339(4)	0.0370(3)	0.0367(2)	0.0367(3)	
B (O2) (Å^2)	1.19(8)	1.80(6)	2.14(4)	2.09(4)	2.19(5)	
R_p (%)	12.0	8.94	4.66	4.69	5.23	4.72
R_{wp} (%)	17.1	12.5	6.11	6.09	7.42	6.21
χ^2	46.8	12.5	2.94	2.92	3.57	2.98
R_{Bragg} (%)	13.3	13.2	6.39	6.50	7.90	6.27

TABLE II. Structural parameters obtained by Rietveld refinements of the neutron powder diffraction data of $La_{1-x}Sr_xMnO_3$ for $x=0.075$ at several temperatures.

	$La_{1-x}Sr_xMnO_3$, $x=0.075$						
Space group	*Pbnm*	*Pbnm*	*Pbnm*	*Pbnm*	*Pbnm*	$R\bar{3}c$	$R\bar{3}c$
T (K)	295	423	473	573	623	673	873
a (Å)	5.5349(2)	5.5397(2)	5.5426(2)	5.5552(1)	5.5604(1)	5.5704(2)	5.58015(9)
b (Å)	5.6263(2)	5.6046(2)	5.5835(2)	5.5332(1)	5.5321(2)		
c (Å)	7.7073(2)	7.7448(2)	7.7737(3)	7.8337(2)	7.8389(2)	13.4612(5)	13.5101(2)
x (La)	−0.0045(4)	−0.0053(5)	−0.0049(6)	−0.0026(6)	−0.0030(5)		
y (La)	0.0356(3)	0.0321(4)	0.0294(4)	0.0200(3)	0.0190(4)		
B (La) (Å^2)	0.97(3)	1.00(3)	1.06(4)	1.00(3)	0.98(3)	1.48(5)	1.41(3)
B (Mn) (Å^2)	0.57(6)	0.81(6)	0.73(7)	0.68(4)	0.75(5)	0.97(9)	1.10(5)
x (O1)	0.0692(5)	0.0668(5)	0.0686(6)	0.0673(6)	0.0672(6)	0.4452(4)	0.4452(2)
y (O1)	0.4903(5)	0.4913(5)	0.4924(6)	0.4918(6)	0.4916(7)		
B (O1) (Å^2)	1.20(5)	1.25(5)	1.29(5)	1.61(6)	1.66(6)	2.48(5)	2.53(3)
x (O2)	0.7284(4)	0.7300(5)	0.7301(6)	0.7274(4)	0.7278(4)		
y (O2)	0.2947(3)	0.2920(4)	0.2870(4)	0.2768(4)	0.2757(4)		
z (O2)	0.0361(2)	0.0364(3)	0.0347(3)	0.0355(3)	0.0348(3)		
B (O2) (Å^2)	1.30(3)	1.58(4)	1.43(4)	1.39(4)	1.47(4)		
R_p (%)	7.04	6.57	7.26	5.64	5.88	7.55	4.86
R_{wp} (%)	8.98	8.65	9.86	7.14	7.42	10.9	6.14
χ^2	6.49	5.87	7.52	3.97	4.27	9.12	2.86
R_{Bragg} (%)	10.4	9.05	9.54	7.59	8.29	9.46	6.92

the Institut Laue-Langevin in Grenoble using monochromatic neutrons of wavelength of 1.59 Å. The FULLPROF program was used to analyze the data using the Rietveld method.

The structural phase transitions in stoichiometric $LaMnO_3$ have been investigated by Rodriguez-Carvajal *et al.*[7] The room-temperature structure of $LaMnO_3$ belongs to the orthorhombic O' phase belonging to the *Pbnm* space group. At

TABLE III. Structural parameters obtained by Rietveld refinements of the neutron powder diffraction data of $La_{1-x}Sr_xMnO_3$ for $x=0.10$ at several temperatures.

	$La_{1-x}Sr_xMnO_3$, $x=0.10$					
Space group	*Pbnm*	*Pbnm*	*Pbnm*	*Pbnm*	*Pbnm*	$R\bar{3}c$
T (K)	294	373	473	523	573	873
a (Å)	5.5375(2)	5.5393(2)	5.5472(2)	5.5526(1)	5.5589(3)	5.5729(1)
b (Å)	5.5975(2)	5.783(2)	5.5309(2)	5.5251(1)	5.5248(3)	
c (Å)	7.7214(2)	7.7533(3)	7.8160(2)	7.8263(2)	7.8302(4)	13.5125(3)
x (La)	−0.0057(4)	−0.0049(5)	−0.0027(5)	−0.0032(4)	−0.0014(11)	
y (La)	0.0329(3)	0.0285(4)	0.0205(3)	0.0183(3)	0.0174(8)	
B (La) (Å^2)	0.92(3)	0.99(4)	1.08(3)	0.99(2)	1.16(6)	1.41(3)
B (Mn) (Å^2)	0.58(5)	0.70(6)	0.71(5)	0.70(4)	0.35(9)	1.12(6)
x (O1)	0.0664(5)	0.0675(6)	0.0659(5)	0.0657(4)	0.0629(10)	0.4465(2)
y (O1)	0.4919(5)	0.4928(6)	0.4936(6)	0.4917(5)	0.4913(14)	
B (O1) (Å^2)	1.27(5)	1.43(5)	1.58(5)	1.60(4)	1.40(10)	2.49(3)
x (O2)	0.7309(4)	0.7304(5)	0.7288(5)	0.7296(3)	0.7400(16)	
y (O2)	0.2904(3)	0.2868(4)	0.2768(4)	0.2750(3)	0.2734(9)	
z (O2)	0.0363(2)	0.0346(3)	0.0352(2)	0.0350(2)	0.0354(5)	
B (O2) (Å^2)	1.33(4)	1.55(4)	1.75(4)	1.59(3)	2.12(9)	
R_p (%)	6.37	6.92	5.36	4.90	8.61	5.46
R_{wp} (%)	8.36	9.33	7.20	6.31	13.2	6.78
χ^2	5.29	6.57	3.92	3.00	13.3	3.48
R_{Bragg} (%)	8.63	9.31	6.30	6.15	14.6	7.26

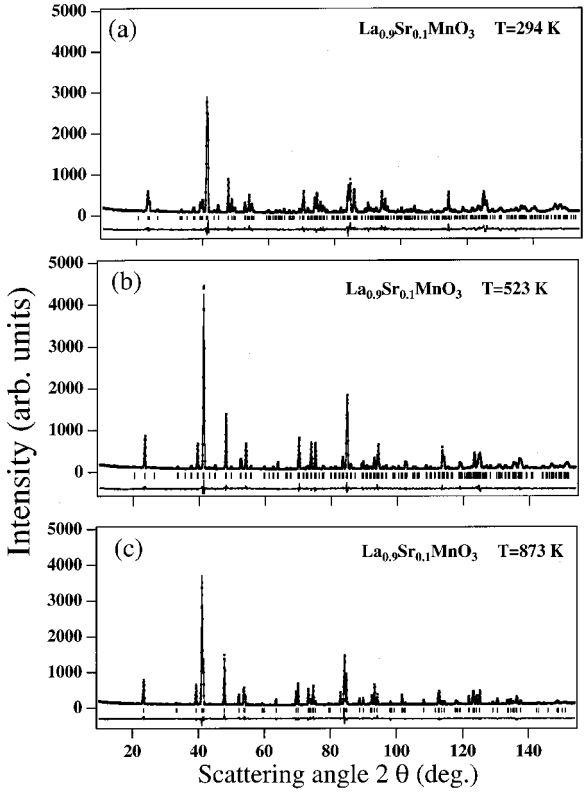

FIG. 2. Observed and calculated powder diffraction patterns of $La_{0.90}Sr_{0.10}MnO_3$ at (a) $T=294$ K in the orthorhombic O' phase, (b) at $T=523$ K in the orthorhombic O phase, and (c) at $T=873$ K in the rhombohedral R phase.

$T_{JT}\approx 750$ K, $LaMnO_3$ undergoes a Jahn-Teller transition to the orthorhombic O phase with the same *Pbnm* space group. The O' phase is orbitally ordered and has Jahn-Teller distortions. The distortion decreases with increasing temperature and becomes very small above T_{JT} in the O phase. The O phase is orbitally disordered. At higher temperature the O phase transforms into the rhombohedral R phase with the space group $R\bar{3}c$. We have investigated the temperature variation of the crystal structure of $La_{1-x}Sr_xMnO_3$ in the small doping range ($0<x\leqslant 0.1$). Tables I–III show the results of structure refinements at several temperatures for the three sample $x=0.05$, 0.075, and 0.10. The room-temperature crystal structure of all the three samples is orthorhombic (O' phase, space group *Pbnm*). At higher temperatures the sequence of the structural transition O'-O-R takes place as in the case of $LaMnO_3$. The O phase has the same orthorhombic *Pbnm* space group as O' and the rhombohedral R phase has the space group $R\bar{3}c$. Figure 2 shows the observed and calculated intensities and their difference for $La_{0.90}Sr_{0.10}MnO_3$ at $T=294$, 523, and 873 K belonging to the O', O, and R phases, respectively, as examples of the quality of structural refinements. Figure 3 shows the temperature variation of the lattice parameters. The lattice parameter a (space group *Pbnm*) increases slowly with increasing temperature, whereas the lattice parameter b decreases strongly. The lattice parameter c increases strongly with increasing temperature. To compare with a and b we have ac-

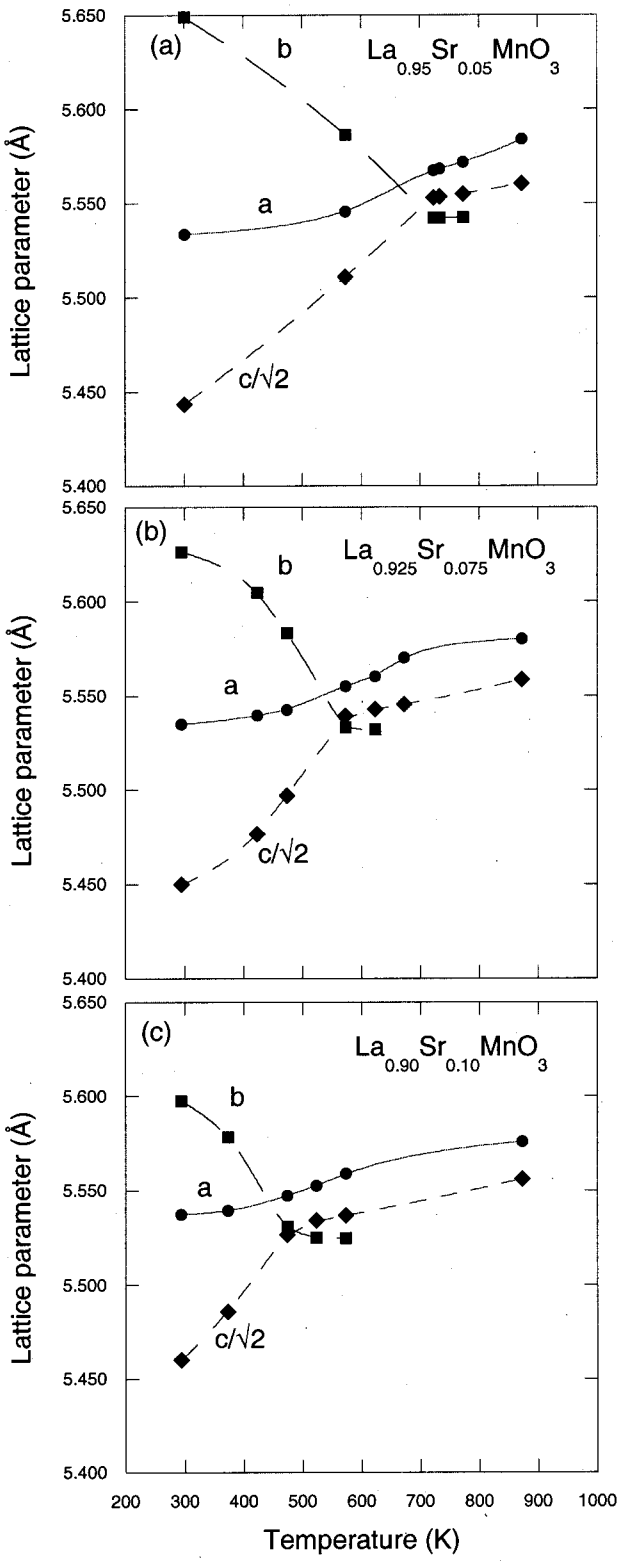

FIG. 3. Temperature variation of the lattice parameters of $La_{1-x}Sr_xMnO_3$ for (a) $x=0.05$, (b) 0.075, and (c) 0.10. In order to compare with the orthorhombic c lattice parameters, the hexagonal cell c of the rhombohedral R phase has been divided by a factor of $\sqrt{2}$. The error bars are smaller than the sizes of the data symbols. The lines are only guides to the eye. The figure clearly demonstrates that the orthorhombic O phase of $La_{1-x}Sr_xMnO_3$ is also metrically orthorhombic for $x=0.05$, 0.075, and 0.10.

tually plotted $c/\sqrt{2}$. At or close to T_{JT} the temperature variation curves for a, b, and c cross one another. Below T_{JT}, $c/\sqrt{2}<a<b$, whereas above T_{JT}, $b<c/\sqrt{2}<a$ for all three samples investigated. Unlike in the case of pure $LaMnO_3$,[7] the lattice parameters remain distinct below the orthorhombic-to-rhombohedral (O-R) transition. The O phase is not at all pseudocubic or metrically cubic, but the differences between the lattice parameters are only much reduced compared to the differences in lattice parameters in the O' phase, but are well above experimental errors. The differences between the lattice parameters in the O phase are about the same for $x=0.05$, 0.075, and 0.10. The lattice parameters a and $c/\sqrt{2}$ of the O phase extrapolate very smoothly to the equivalent lattice parameters a and c_{eq} of the rhombohedral R phase (space group $R\bar{3}c$) at higher temperature. This leads us to suspect the ''pseudocubic'' or ''metrically cubic'' description of the O phase. We give below the relationships between the lattice parameters a_O, b_O, and c_O of the orthorhombic and lattice parameters a_H and c_H of the rhombohedral phase in hexagonal setting:

$$\mathbf{a}_H=\mathbf{b}_O, \tag{1}$$

$$\mathbf{b}_H=\frac{1}{2}(\mathbf{a}_O-\mathbf{b}_O-\mathbf{c}_O), \tag{2}$$

$$\mathbf{c}_H=2\mathbf{a}_O+\mathbf{c}_O. \tag{3}$$

The ''equivalent'' $c/\sqrt{2}$ for the rhombohedral phase $c_{eq}=c_O/\sqrt{2}$ can be obtained from the above equations

$$18c_{eq}^2=c_H^2+12a_H^2. \tag{4}$$

The Jahn-Teller transition temperature is increasingly reduced from $T_{JT}\approx 750$ K for $x=0$ to $T_{JT}\approx 475$ K for $x=0.10$. Figure 4(a) shows the temperature variation of the unit cell volume which shows a monotonic increase, but without any anomaly or discontinuity at T_{JT} or at the O-R transition temperature. Figure 4(b) shows the temperature variation of the isotropic thermal parameter B for La, Mn, and O atoms for $La_{1-x}Sr_xMnO_3$ with $x=0.05$. The isotropic thermal parameters of La and Mn increase as a function of temperature as expected. The thermal parameters of oxygen atoms also increase with temperature and become rather large at temperatures above T_{JT}.

The ideal cubic perovskite structure ABX_3, which consists of corner-linked octahedra of X anions with B cations at their centers and A cations between them, is realized only in some materials; more frequently, the structure is modified either by cation displacements, Jahn-Teller distortions of the BO_6 octahedra, or tilting of the octahedra or a combinations of these. The modification of the perovskite structure by tilting of the octahedra has been discussed by several authors.[8–10] The cation displacements in some perovskite cause ferro or antiferroelectric behaviors. More relevant to the present investigations is the distortion of the BO_6 octahedra due to the Jahn-Teller effects caused by the $3d$ Jahn-Teller ions, viz., Cu^{2+} or Mn^{3+} discussed by Kanamori[11] and others.[12] The distortion of the MnO_6 octahedron due to

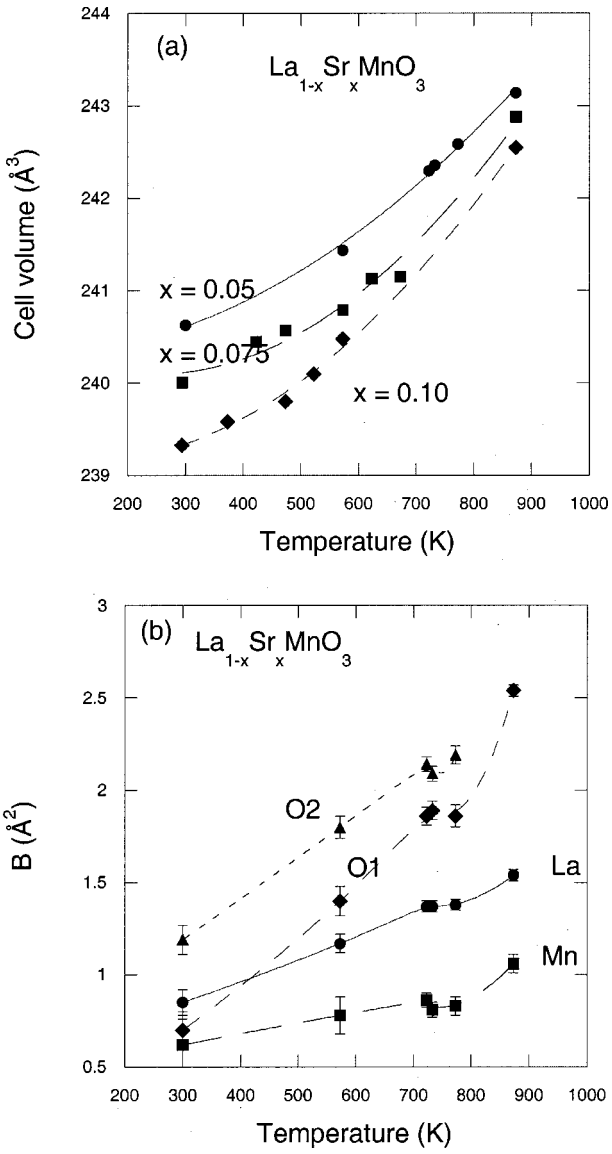

FIG. 4. (a) Temperature variation of the unit cell volume of $La_{1-x}Sr_xMnO_3$ with $x=0.05$, 0.075, and 0.10. In order to compare with the orthorhombic cell volume, the hexagonal cell volume of the rhombohedral R phase has been multiplied by a factor of $\frac{2}{3}$. The lines are only guides to the eye. (b) Temperature variation of the isotropic thermal parameters of La, Mn, and O atoms of $La_{1-x}Sr_xMnO_3$ with $x=0.05$. The lines are only guides to the eye.

the Jahn-Teller effect produces three Mn-O bond distances: long (l), short (s), and medium (m). The distorted crystal structure can be obtained from the ideal perovskite structure in the following way: first, the distortion Q_2 of the octahedron formed with O^{2-} ions is added in a staggered way along the three directions, and then the distortion Q_3 is superposed on it. These two distortion modes are expressed in terms of l,s,m by

$$Q_2=\frac{2}{\sqrt{2}}(l-s), \tag{5}$$

$$Q_3=\frac{2}{\sqrt{6}}(2m-l-s). \tag{6}$$

TABLE IV. Geometrical parameters characterizing Jahn-Teller transitions of MnO_6 octahedra of $La_{1-x}Sr_xMnO_3$ for $x=0.05$ at several temperatures.

	$La_{1-x}Sr_xMnO_3$, $x=0.05$					
Space group	*Pbnm*	*Pbnm*	*Pbnm*	*Pbnm*	*Pbnm*	$R\bar{3}c$
T (K)	300	573	723	733	773	873
Mn-$O_1\times2(m)$ (Å)	1.967(1)	1.990(1)	2.0010(5)	2.0018(5)	2.0019(7)	1.991
Mn-$O_2\times2(s)$ (Å)	1.906(5)	1.913(5)	1.985(2)	1.984(2)	1.976(3)	
Mn-$O_2\times2(l)$ (Å)	2.129(4)	2.083(4)	2.001(2)	2.002(2)	2.009(3)	
$\langle$Mn-O$\rangle=\langle d\rangle$ (Å)	2.001	1.995	1.996	1.996	1.996	
Δ(Mn-O)$\times10^4$	22.12	12.13	0.14	0.18	0.51	
θ_1=Mn-O_1-Mn (deg)	156.3(9)	156.7(7)	157.7(4)	157.5(4)	157.7(2)	161.7(1)
θ_2=Mn-O_2-Mn (deg)	157.0(6)	160.0(4)	160.3(2)	160.5(2)	160.82(9)	
$\langle\phi\rangle$ (deg)	14.27	13.23	12.83	12.83	12.67	11.23
c_2	0.7915	0.7260	0.8660	0.8636	0.8101	
c_1	0.6112	0.6877	0.5000	0.5042	0.5863	

TABLE V. Geometrical parameters characterizing Jahn-teller transitions of MnO_6 octahedra of $La_{1-x}Sr_xMnO_3$ for $x=0.075$ at several temperatures.

	$La_{1-x}Sr_xMnO_3$, $x=0.075$						
Space group	*Pbnm*	*Pbnm*	*Pbnm*	*Pbnm*	*Pbnm*	$R\bar{3}c$	$R\bar{3}c$
T (K)	295	423	473	573	623	673	873
Mn-$O_1\times2(m)$ (Å)	1.9653(5)	1.9718(5)	1.9807(6)	1.9943(6)	1.9952(6)	1.984	1.989
Mn-$O_2\times2(s)$ (Å)	1.916(2)	1.917(2)	1.927(3)	1.974(2)	1.976(2)		
Mn-$O_2\times2(l)$ (Å)	2.104(2)	2.093(2)	2.069(3)	2.005(2)	2.001(2)		
$\langle$Mn-O$\rangle=\langle d\rangle$ (Å)	1.995	1.994	1.992	1.991	1.991		
Δ(Mn-O)$\times10^4$	15.92	13.60	8.63	0.42	0.29		
θ_1=Mn-O_1-Mn (deg)	157.3(5)	158.2(4)	157.7(5)	158.2(5)	158.3(5)	162.3(3)	162.3(3)
θ_2=Mn-O_2-Mn (deg)	158.0(3)	158.5(2)	159.6(3)	160.4(2)	160.8(2)		
$\langle\phi\rangle$ (deg)	13.66	13.24	13.05	12.65	12.50	10.86	10.86
c_2	0.7952	0.7787	0.7548	0.7668	0.8049		
c_1	0.6063	0.6274	0.6560	0.6419	0.5935		

TABLE VI. Geometrical parameters characterizing Jahn-Teller transitions of MnO_6 octahedra of $La_{1-x}Sr_xMnO_3$ for $x=0.10$ at several temperatures.

	$La_{1-x}Sr_xMnO_3$, $x=0.10$					
Space group	*Pbnm*	*Pbnm*	*Pbnm*	*Pbnm*	*Pbnm*	$R\bar{3}c$
T (K)	294	373	473	523	573	873
Mn-$O_1\times2(m)$ (Å)	1.9656(5)	1.9744(6)	1.9882(5)	1.9902(5)	1.990(1)	1.987
Mn-$O_2\times2(s)$ (Å)	1.917(2)	1.928(3)	1.966(3)	1.970(2)	1.935(7)	
Mn-$O_2\times2(l)$ (Å)	2.087(2)	2.064(3)	2.007(3)	2.001(2)	2.032(6)	
$\langle$Mn-O$\rangle$ (Å)	1.990	1.989	1.987	1.987	1.986	
Δ(Mn-O)$\times10^4$	12.91	8.05	0.71	0.41	4.00	
θ_1=Mn-O_1-Mn (deg)	158.3(4)	158.1(4)	158.7(4)	158.9(3)	159.4(9)	162.7(2)
θ_2=Mn-O_2-Mn (deg)	158.9(2)	159.9(3)	160.7(2)	161.2(2)	162.1(5)	
$\langle\phi\rangle$ (deg)	13.08	12.84	12.41	12.19	11.77	10.61
c_2	0.7874	0.7682	0.7238	0.7657	0.7339	
c_1	0.6164	0.6402	0.6900	0.6433	0.6793	

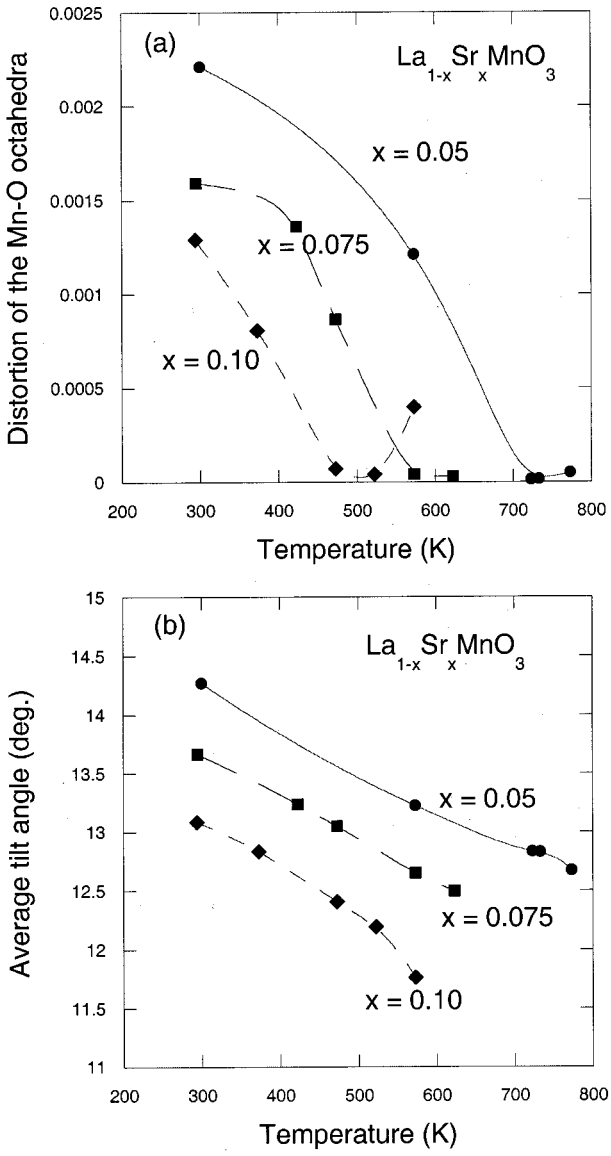

FIG. 5. (a) Temperature variation of the distortion Δ of the MnO_6 octahedron of $La_{1-x}Sr_xMnO_3$ for $x=0.05$, 0.075, and 0.10. The octahedral distortion is reduced to a very small value at the O'-O phase transition. The distortion is also reduced with hole doping. The lines are only guides to the eye. (b) Temperature variation of the average tilt angle of the MnO_6 octahedra around the pseudocubic [111] direction of $La_{1-x}Sr_xMnO_3$ for $x=0.05$, 0.075, and 0.10. The average tilt angle decreases with increasing temperature; it does not show any drastic decrease at the O'-O transition, showing that this transition is not caused by steric effects. The lines are only guides to the eye.

The ground-state wave functions are given by

$$\Psi_g = c_1\phi_{x^2-y^2} + c_2\phi_{3z^2-r^2} \tag{7}$$

$$\Psi_e = c_1\phi_{x^2-y^2} - c_2\phi_{3z^2-r^2}. \tag{8}$$

The coefficients c_1 and c_2 which satisfy the condition

$$c_1^2 + c_2^2 = 1 \tag{9}$$

can be obtained from the equations

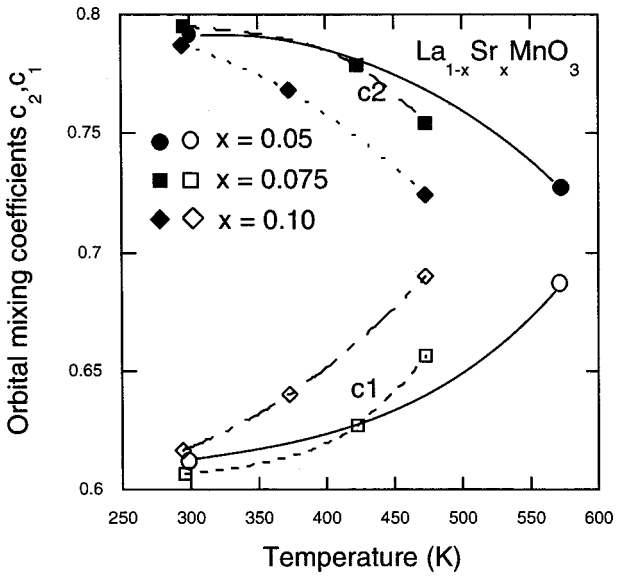

FIG. 6. Temperature variation of the orbital mixing coefficients c_1 and c_2 of $La_{1-x}Sr_xMnO_3$ for $x=0.05$, 0.075, and 0.10. The lines are only guides to the eye.

$$\tan\Phi = \frac{Q_2}{Q_3}, \tag{10}$$

$$\tan\frac{\Phi}{2} = \frac{c_1}{c_2}. \tag{11}$$

Tables IV–VI give geometrical parameters related to the Jahn-Teller effect at different temperatures for $La_{1-x}Sr_xMnO_3$ with $x=0.05$, 0.075, and 0.10. The three bond distances m,s,l are tabulated along with the average $\langle$Mn-O$\rangle$ bond distances. The distortion parameter Δ of a coordination polyhedron BO_N with an average B-O distance $\langle d\rangle$ is defined as

$$\Delta = \frac{1}{N}\sum_{n=1,N}\left\{\frac{d_n - \langle d\rangle}{\langle d\rangle}\right\}^2. \tag{12}$$

From Tables IV–VI we note that the distortion Δ of the octahedron diminishes with increasing temperature for all three samples. The distortion is drastically reduced on approaching T_{JT}. The three Mn-O bond distances (m,s,l) approach almost the same value. However, the distortion is not completely removed; the crystal structure retains the orthorhombic *Pbnm* symmetry, and the lattice remains still metrically orthorhombic. The distortion Δ of the MnO_6 octahedra at a particular temperature is reduced with increasing doping x. Figure 5(a) shows the distortion Δ as a function of temperature for $x=0.05$, 0.075, and 0.10. At higher temperature the measurement of Δ is not very accurate due to its drastic reduction and the values are not at all meaningful.

The two Mn-O-Mn angles θ_1 and θ_2 are related[10] to the tilt angle φ of the MnO_6 octahedra around the pseudocubic [111] direction by the equations

$$\cos\theta_1 = \frac{2-5\cos^2\varphi_1}{2+\cos^2\varphi}, \tag{13}$$

$$\cos\theta_2 = \frac{1-4\cos^2\varphi_2}{3}. \tag{14}$$

Tables IV–VI give the average $\langle\varphi\rangle$ obtained from φ_1 and φ_2. Tables IV–VI give the orbital mixing coefficients c_1 and c_2 at different temperatures for $La_{1-x}Sr_xMnO_3$ with $x=0.05$, 0.075, and 0.10. Figure 5(b) shows the average tilt angle of the MnO_6 octahedra around the pseudocubic [111] direction as function of temperature. The average tilt angle decreases with increasing temperature. It does not show any drastic decrease at the O'-O transition, but the tilt angle is very much reduced in the rhombohedral phase. The fact that the average octahedral tilt does not show any drastic change at the O'-O transition indicates that the transition is not driven by merely a steric effect, but is driven by orbital ordering. On the other hand the O-R transition is probably driven by steric effects only.

Figure 6 shows the temperature variation of the orbital mixing coefficients c_1 and c_2. It is difficult to determine the standard deviations of c_1 and c_2, but they are estimated to be of the order of 0.1 at the maximum. It is to be noted that due to the reduced distortion no meaningful values of the orbital mixing coefficients could be extracted at higher temperatures than have been shown in Fig. 6. The values of the orbital mixing coefficients c_1 and c_2 corresponding to the $d_{x^2-y^2}$ and $d_{3z^2-r^2}$ orbitals in the O' phase at room temperature are about 0.61 and 0.79, respectively, for all the three samples. These values are about the same as that obtained by Rodriguez-Carvajal *et al.*[7] for the stoichiometric $LaMnO_3$ at room temperature. We recall that we get $d_{3x^2-r^2}$ and $d_{3y^2-r^2}$ orbitals from the basis $d_{x^2-y^2}$ and $d_{3z^2-r^2}$ by the mixing coefficients $c_1=\frac{1}{2}=0.5$ and $c_2=\sqrt{3}/2=0.866$. So the orbitals in $La_{1-x}Sr_xMnO_3$ are almost, but not completely ordered at room temperature. Figure 6 shows that the experimentally determined values of c_1 and c_2 approach 0.71 if they are extrapolated to the respective T_{JT}. This is what is expected ($c_1=c_2=1/\sqrt{2}=0.7071$) for the orbitally disordered state above T_{JT}. The equalization of the mixing coefficients is, however, not complete. This leads probably to the noncubic lattice parameters in the O phase and also should give rise to short-range orbital order. Charge fluctuations due to the short-range orbital order should exist above T_{JT} and can possibly be probed by light scattering experiments. Indeed, such charge fluctuations have been observed in bilayer manganites.[13]

In conclusion, our investigations of the high-temperature structural phase transitions in $La_{1-x}Sr_xMnO_3$ with $x=0.05$, 0.075, and 0.10 show similar behavior as that of stoichiometric $LaMnO_3$. The only difference is that, unlike the orthorhombic O phase of $LaMnO_3$, the orthorhombic O phase in the lightly doped compounds above T_{JT} is metrically orthorhombic. The Jahn-Teller transition temperature T_{JT} decreases drastically with doping from $T_{JT}\approx 750$ K to $T_{JT}\approx 700$, 575, and 475 K for $x=0.05$, 0.075, and 0.10, respectively. The O-R transition temperature is also similarly reduced with doping. Due to the lack of neutron beam time, we could not determine the transition temperatures precisely. The results are in qualitative agreement with a recent resistivity investigation[5] of $La_{1-x}Sr_xMnO_3$ in the low-doping range.

[1] *Colossal Magnetoresistive Oxides*, edited by Y. Tokura (Gordon and Breach, New York, 2000).

[2] *Colossal Magnetoresistance, Charge Ordering and Related Properties of Manganese Oxides*, edited by C. N. R. Rao and B. Raveau (World Scientific, Singapore, 1998).

[3] J. M. D. Coey, M. Viret, and S. von Molnar, Adv. Phys. **48**, 167 (1999).

[4] A. P. Ramirez, J. Phys.: Condens. Matter **9**, 8171 (1997).

[5] P. Mandal, B. Bandyapadhyav, and B. Ghosh, Phys. Rev. B **64**, 180405(R) (2001).

[6] Y. Murakami, J. P. Hill, D. Gibbs, M. Blume, I. Koyama, M. Tanaka, H. Kawata, T. Arima, Y. Tokura, K. Hirota, and Y. Endoh, Phys. Rev. Lett. **81**, 582 (1998).

[7] J. Rodriguez-Carvajal, M. Hennion, F. Moussa, A. H. Moudden, L. Pinsard, and A. Revcolevschi, Phys. Rev. B **57**, R3189 (1998).

[8] A. M. Glazer, Acta Crystallogr., Sect. B: Struct. Crystallogr. Cryst. Chem. **28**, 3384 (1972).

[9] A. M. Glazer, Acta Crystallogr., Sect. B: Struct. Crystallogr. Cryst. Chem. **28**, 3384 (1972).

[10] M. O'Keeffe and B. G. Hyde, Acta Crystallogr., Sect. B: Struct. Crystallogr. Cryst. Chem. **33**, 3802 (1977).

[11] J. Kanamori, J. Appl. Phys. **31**, 14S (1960).

[12] G. Matsumoto, J. Phys. Soc. Jpn. **29**, 606 (1970).

[13] D. N. Argyriou, H. N. Bordallo, B. J. Campbell, A. K. Cheetham, D. E. Cox, J. S. Gardner, K. Hanif, A. dos Santos, and G. F. Strouse, Phys. Rev. B **61**, 15 269 (2000).